

# Impact of Environmental Conditions on Grass Phenology in the Regional Climate Model COSMO-CLM

Eva Nowatzki<sup>1</sup>, Jan-Peter Schulz<sup>2</sup>, Ruben Seibert<sup>3</sup>, Marius Schmidt<sup>4</sup>, Mingyue Zhang<sup>1</sup>,  
Jürg Luterbacher<sup>1</sup>, and Merja Tölle<sup>1</sup>

<sup>1</sup>Department of Geography, Climatology, Climate Dynamics and Climate Change,  
Justus-Liebig University Giessen, Giessen, Germany

<sup>2</sup>Deutscher Wetterdienst (DWD, German Meteorological Service), Offenbach, Germany

<sup>3</sup>Department of Biology, Plant Ecology, Justus-Liebig University Giessen, Giessen,  
Germany

<sup>4</sup>Institute of Bio- and Geosciences, Agrosphere (IBG-3), Forschungszentrum Jülich, Jülich,  
Germany

November 22, 2022

## Abstract

Phenology and its interannual variability are altered through anthropogenic climate change. Feedbacks of plant phenology to the regional climate system affect fluxes of energy, water, CO<sub>2</sub>, biogenic volatile organic compounds as well as canopy conductance, surface roughness length, and are influencing the seasonality of albedo. We performed simulations with the regional climate model COSMO-CLM (CCLM) with 3km horizontal resolution over Germany covering the period 1999 to 2015 to study the sensitivity of grass phenology to different environmental conditions by implementing a new phenology module. We provide new evidence that the standard annually-recurring phenology of CCLM is improved by the new calculation of leaf area index (LAI) dependent upon surface temperature, day length, and water availability. Results with the new phenology implemented in the model showed a significantly higher correlation with observations than simulations with the standard phenology. The interannual variability of LAI, the representation of years with extremely warm spring or extremely dry summer, and the start of the growing season also improved with the new phenology module. The number of hot days with maximum temperature exceeding the 90th percentile and heavy precipitation events (> 20mm) with the new phenology are in very good agreement with the observations. We also show that lower LAI values in summer lead to a decrease of latent heat flux in the model due to less evapotranspiration. The CCLM simulation with improved representation of the phenology should be used in future applications with an extension on more plant functional types.

1                   **Impact of Environmental Conditions on Grass**  
2                   **Phenology in the Regional Climate Model**  
3                   **COSMO-CLM**

4                   **Eva Nowatzki<sup>1</sup>, Jan-Peter Schulz<sup>2</sup>, Ruben Seibert<sup>3</sup>, Marius Schmidt<sup>4</sup>,**  
5                   **Mingyue Zhang<sup>1</sup>, Jürg Luterbacher<sup>1,5</sup>, and Merja Tölle<sup>1</sup>**

6                   <sup>1</sup>Department of Geography, Climatology, Climate Dynamics and Climate Change, Justus-Liebig

7                   University Giessen, Giessen, Germany

8                   <sup>2</sup>Deutscher Wetterdienst (DWD, German Meteorological Service), Offenbach, Germany

9                   <sup>3</sup>Department of Biology, Plant Ecology, Justus-Liebig University Giessen, Giessen, Germany

10                  <sup>4</sup>Institute of Bio- and Geosciences, Agrosphere (IBG-3), Forschungszentrum Jülich, Jülich, Germany

11                  <sup>5</sup>World Meteorological Organization (WMO), Science and Innovation Department, Geneva, Switzerland

12                  **Key Points:**

- 13                  • COSMO-CLM simulations with phenology depending on surface temperature, day  
14                  length, and water availability show a significant improvement of the mean annual  
15                  cycle of LAI in experiments over Germany covering the period 1999-2015.
- 16                  • Years with an extremely warm winter/spring or an extremely dry summer affect  
17                  interannual variations of LAI with an earlier start of the growing season or reduced  
18                  LAI due to lack of water in the simulations with the new phenology in very good  
19                  agreement with the observations.
- 20                  • Changes in LAI of grass influence the number of extreme hot/wet days and the  
21                  transpiration rate, resulting in enhanced simulated latent heat flux.

---

Corresponding author: Eva Nowatzki, [eva.nowatzki@geogr.uni-giessen.de](mailto:eva.nowatzki@geogr.uni-giessen.de)

## Abstract

Phenology and its interannual variability are altered through anthropogenic climate change. Feedbacks of plant phenology to the regional climate system affect fluxes of energy, water, CO<sub>2</sub>, biogenic volatile organic compounds as well as canopy conductance, surface roughness length, and are influencing the seasonality of albedo. We performed simulations with the regional climate model COSMO-CLM (CCLM) with 3 km horizontal resolution over Germany covering the period 1999 to 2015 to study the sensitivity of grass phenology to different environmental conditions by implementing a new phenology module. We provide new evidence that the standard annually-recurring phenology of CCLM is improved by the new calculation of leaf area index (LAI) dependent upon surface temperature, day length, and water availability. Results with the new phenology implemented in the model showed a significantly higher correlation with observations than simulations with the standard phenology. The interannual variability of LAI, the representation of years with extremely warm spring or extremely dry summer, and the start of the growing season also improved with the new phenology module. The number of hot days with maximum temperature exceeding the 90th percentile and heavy precipitation events (> 20 mm) with the new phenology are in very good agreement with the observations. We also show that lower LAI values in summer lead to a decrease of latent heat flux in the model due to less evapotranspiration. The CCLM simulation with improved representation of the phenology should be used in future applications with an extension on more plant functional types.

## 1 Introduction

Phenology is the timing of seasonal activities of animals and plants (Schnelle, 1955; Walther et al., 2002). It indicates changes in ecology (Walther et al., 2002) which are linked to local or regional climate variability (Parmesan, 2006). Phenology is also affected by climate change (Parmesan & Yohe, 2003; Settele et al., 2014), since the 1950s, the growing season in temperate Europe lengthened by 3.6 days per decade (Menzel & Fabian, 1999; Walther et al., 2002; Jeong et al., 2011). With higher CO<sub>2</sub> concentrations and warmer conditions, the growing season will further extend (Reyes-Fox et al., 2014).

The phenology mainly depends on the vegetation type, but also temperature and precipitation influence the phenological stages (White et al., 1997). Additionally, the length of the photoperiod (day length) plays an important role, and together with temperature influences the length of the growing period (Heide, 1974; Oleksyn et al., 1992). The precipitation and the available soil water are important for the variability during the phenophase (Hodges, 1991). Years with an exceptional course of phenology are also associated with extreme temperature and/or precipitation (Shen et al., 2011). When a year starts with an anomalous warm winter and spring, the vegetation usually also starts growing earlier, and later when winter/spring is cold. The end of the growing season is usually earlier when the late summer or autumn is colder than usual, and later when it is warm (Chmielewski & Rötzer, 2002). Precipitation as a source for soil water has a strong influence on the development of the leaf area index (LAI, the leaf area per unit area of land (Watson, 1947)) especially in summer during the growing season (Currie & Peterson, 1966). The more precipitation occurs the more water is available for the plants. In a year with less precipitation, there is less water available thus a reduction of the LAI is observed (Gilgen & Buchmann, 2009).

Inversely, the energy and water cycle of the regional climate is influenced by the phenological development of the vegetation through albedo, and sensible and latent heat flux changes (Peñuelas et al., 2009). This influences near-surface air temperature, precipitation, and ultimately the boundary layer structure. The impact of vegetation on the weather and climate conditions (Collatz et al., 2000; Tölle et al., 2014) are most visible in extreme events as the 2003 European summer heatwaves (Stéfanon et al., 2012). Higher insolation in spring enhances evapotranspiration in June leading to land surface cooling, whereas in August the evapotranspiration is reduced by water stress leading to an

75 early leave fall (Stéfanon et al., 2012). The sensitivity of latent heat flux to vegetation  
 76 is shown in Yang et al. (1999); Peñuelas et al. (2009); I. N. Williams and Torn (2015)  
 77 and is already validated for different land-surface models (Flerchinger et al., 1998; Na-  
 78 gai, 2003; Best & Grimmond, 2016).

79 Phenology and associated vegetation dynamics are accounted for in many differ-  
 80 ent land surface models and still need improvements (Richardson et al., 2013). Main ex-  
 81 amples are the Community-Land Model (CLM) (Oleson et al., 2013), the Lund-Potsdam-  
 82 Jena (LPJ) (Sitch et al., 2003) and ORCHIDEE (Ryder et al., 2014). These sophisti-  
 83 cated land surface models are coupled to many regional climate models. The computa-  
 84 tional costs are very high and the horizontal resolution of the grid is rather coarse ( $\sim$   
 85  $12 - 50$  km). High horizontal resolution ( $\sim 1 - 3$  km) and less computational demand  
 86 can be achieved through less complex models. For example, the regional climate model  
 87 COSMO-CLM (CCLM) is used for applications at a convection-permitting scale with  
 88 the land surface model TERRA-ML (Doms et al., 2011; Schulz et al., 2016). It is a land-  
 89 surface model of the second generation using the so-called BATS model (Dickinson, 1984)  
 90 or the simpler Bucket model (Manabe, 1969). In CCLM, the phenology is static and does  
 91 not depend on the environmental conditions. It follows a sinusoidal cycle depending on  
 92 the geographical latitude and altitude (Doms et al., 2011; Schättler & Blahak, 2017). Be-  
 93 cause those are constants, the annual cycle is every year the same for each simulated lo-  
 94 cation. The annual cycle of LAI starts with the growth of the vegetation in spring and  
 95 ends with the senescence in autumn. Those events differ from year to year in nature and  
 96 should therefore also in the model do so. Vegetation-atmosphere interactions need to be  
 97 accurately represented in regional climate models to improve projections. The static annually-  
 98 recurring phenology is in contradiction to the changing phenological cycle due to climate  
 99 change that is observed. The CCLM is neither able to simulate the interannual variabil-  
 100 ity of vegetation nor the feedbacks between climate and vegetation. Therefore, the model  
 101 needs to be improved through phenology susceptible to environmental conditions. Mod-  
 102 els calculating phenology based on temperature give better results compared to satel-  
 103 lite observations than models with complex photosynthetic modules (Murray-Tortarolo  
 104 et al., 2013). That is why a calculation of phenology based on temperature is chosen (Knorr  
 105 et al., 2010).

106 The main objective of this study is to implement a new phenology calculation for  
 107 grassland in the CCLM model. The new phenology depends on the surface temperature,  
 108 the day length, and the water availability, allowing for interannual variability of the LAI.  
 109 We will examine three experimental areas in Germany from 1999 to 2015. The simulated  
 110 mean annual cycle and the annual cycle of extreme years of LAI will be compared to ob-  
 111 servations. Further, the influence of phenology on extreme events of temperature and  
 112 precipitation will be studied. Additionally, the impact of the phenology on the latent heat  
 113 flux in the CCLM model will be evaluated in this study. To assess the performance of  
 114 this new phenology, the following research questions will be addressed:

- 115 1. How is the annual cycle of LAI affected by the newly implemented phenology?
- 116 2. Does the representation of extreme events in CCLM change with the new phenol-  
 117 ogy module?
- 118 3. What is the influence of the phenology on atmospheric variables, such as temper-  
 119 ature, precipitation, and moisture?

## 120 **2 Data and Methods**

### 121 **2.1 Meteorological Observations**

122 The three experimental domains are chosen to be at locations with observational  
 123 sites (figure 1). The Lindenberg Meteorological Observatory (station ID 03015) is oper-  
 124 ated by the German Meteorological Service (Deutscher Wetterdienst, DWD) (Neisser et  
 125 al., 2002). Temperature and precipitation data are freely available. At Linden is the mea-

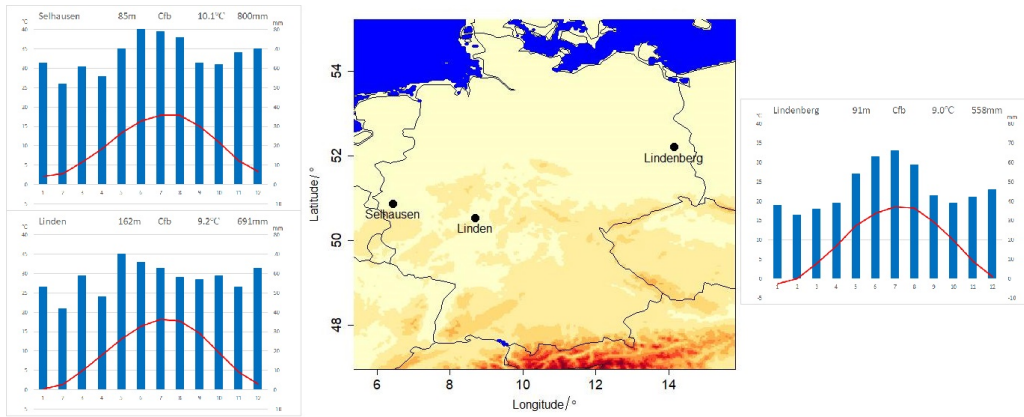


**Figure 1.** The map with the three experimental locations (Lindenberg, Linden, and Selhausen) surrounded by their climate diagrams (data from Merkel (2020), 1982-2012).

126 suring station of the University of Giessen for the GiFACE project (Jäger et al., 2003;  
 127 Andresen et al., 2018). Besides the meteorological measurements of temperature and pre-  
 128 cipitation, leaf area index measurements are available for individual years. The exper-  
 129 imental crop site of Selhausen is operated by the Institute of Bio- and Geosciences, Agro-  
 130 sphere (IBG-3) of the Forschungszentrum Jülich (Post et al., 2018; Bogena et al., 2018).  
 131 Measurements of leaf area index and air temperature from the site were available at the  
 132 CRC/TR32 database (<https://www.tr32db.uni-koeln.de>) or the TERENO data portal  
 133 (<http://www.tereno.net/ddp/>). In addition, precipitation data from the DWD station  
 134 Jülich (02473) is included. The station data will be used to find extremely warm/dry  
 135 years.

136 Precipitation and temperature information is also taken from HYRAS, a high-resolution  
 137 gridded daily data set with 5 km spatial and a daily temporal resolution (Rauthe et al.,  
 138 2013). The HYRAS data set is calculated from the information of approximately 6200  
 139 stations including the DWD stations using the REGNIE method, a combination of mul-  
 140 tiple linear regression considering orographical conditions and inverse distance weight-  
 141 ing (Rauthe et al., 2013). This daily gridded data set will be used to derive heavy pre-  
 142 cipitation and hot temperature events. The threshold for heavy precipitation amount  
 143 at a certain time is set to 20 mm per day (Kundzewicz et al., 2006; Bartholy & Pongrácz,  
 144 2007). An extremely hot day is defined as a day within the 90th percentile of maximum  
 145 temperature (Yan et al., 2002; González-Aparicio & Hidalgo, 2012).

## 146 2.2 LAI Measurements

147 Indirect methods based on radiation measurements are applied to measure the LAI.  
 148 The indirect method is not as precise as the direct method (collect leaves and measure  
 149 their area) but can easily be automated and is less expensive and complex (Cutini et al.,  
 150 1998). One of the common indirect methods is the plant canopy analyzer LAI-2000 (Li-  
 151 Cor, 1992) or the SunScan SS1 LAI meter (Delta-T Devices Ltd, Cambridge, UK). Here  
 152 LAI is determined by measuring the light extinction in a canopy that is related to LAI.  
 153 The indirect method is used at Linden and Selhausen to obtain the leaf area index. The  
 154 measurements are made over grassland covering an area of about 100 m x 200 m in Lin-  
 155 den from 1998 to 2002 (Kammann et al., 2005) and from 2014 to 2016 and in Selhausen  
 156 from 2016 to 2018 over crops (2016: barley followed by greening mix, 2017: sugar beet,  
 157 2018: winter wheat).

158 We also use satellite observed leaf area index data because in-situ measurements  
 159 are very sparse regarding spatial and temporal resolution. The LAI is calculated from

160 the satellite product of SPOT and PROBA-V (Smets et al., 2019), derived from the nor-  
 161 malized reflectance of red, near-infrared, and shortwave-infrared radiation (Verger et al.,  
 162 2014). Because the vegetation is not equally distributed in reality it comes to an irreg-  
 163 ular distribution of the plants within remote sensing products (clumping). Therefore,  
 164 this product uses a method to distribute the vegetation equally in the resolved grid (Chen  
 165 et al., 2005). The data is provided by the University of Hamburg with a horizontal res-  
 166 olution of 1 km and a temporal resolution of 10 days from 1999 to 2015 (Baret et al., 2013;  
 167 Camacho et al., 2013). For comparison with the simulations, one grid cell of the grid-  
 168 ded leaf area index will be used at each experimental domain. One pixel of the satellite  
 169 data is 50 times larger than the area of the in-situ measurements. This means that there  
 170 is not only grass in this pixel but also other vegetation types including forests and crops  
 171 and non-vegetated surfaces (urban areas). The LAI measurements from the FACE (Jäger  
 172 et al., 2003; Andresen et al., 2018) and the Tereno project (Post et al., 2018; Bogena et  
 173 al., 2018) will be used to validate the satellite observations at the two specific areas be-  
 174 cause in-situ measurements of LAI have much more precise results at a specific location  
 175 but cover a limited area and time. The satellite observations will finally be used to eval-  
 176 uate the simulations at the three locations and for the whole period.

### 177 2.3 COSMO-CLM

178 The simulations will be performed with the regional climate model COSMO-CLM  
 179 (Rockel et al., 2008) in single column mode. COSMO-CLM is the model of the COnsortium  
 180 for Small-scale MOdelling (COSMO) in CLimate Mode (Baldauf et al., 2011; Rockel  
 181 et al., 2008) and is the community model of the German regional climate research com-  
 182 munity jointly further developed by the CLM-Community. The COSMO model version  
 183 5.0 with CLM version 15 (COSMO-CLM – *v5.0\_clm15*) is used. The Interpolation is  
 184 done with INT2LM in version 2.05 with CLM version 1 (INT2LM–*v2.05\_clm1*) (Schättler  
 185 & Blahak, 2017). The time-integration is the two time-level Runge-Kutta scheme (Jameson  
 186 et al., 1981) and the model time step is 25 seconds. Following convection-permitting sim-  
 187 ulations in general, only the shallow convection parameterization based on the Tiedtke  
 188 scheme (Tiedtke, 1988) is used. The land surface model is TERRA-ML (Doms et al., 2011;  
 189 Schulz et al., 2016). It is a multi-layer scheme that computes temperature and water con-  
 190 tent on 10 soil layers. The bare soil evaporation and the transpiration by plants are sim-  
 191 ulated following the BATS scheme (Dickinson, 1984), together they form the evapotran-  
 192 spiration. The transpiration is based on a Jarvis (1976)-type formulation depending on  
 193 several environmental stress factors, taking into account the LAI. The simulations are  
 194 forced with ERA-Interim reanalysis data (Dee et al., 2011). The leaf area index, root  
 195 depth, and vegetation area fraction in the external data file are adjusted to grassland.  
 196 In this way, the simulations can be compared without being influenced by differences in  
 197 land coverage.

198 The horizontal resolution of the simulations will be  $0.0275^\circ$ , which is about 3 km.  
 199 Three specific experimental domains are chosen, depending on the location of the ob-  
 200 servational sites in Germany. Those are Lindenberg ( $Lat = 52.220^\circ$ ,  $Lon = 14.135^\circ$ ,  
 201  $Alt = 91$  m) in Brandenburg, Linden ( $Lat = 50.531^\circ$ ,  $Lon = 8.704^\circ$ ,  $Alt = 162$  m)  
 202 close to Giessen in Hesse and Selhausen ( $Lat = 50.855^\circ$ ,  $Lon = 6.439^\circ$ ,  $Alt = 85$  m)  
 203 close to Jülich in North Rhine-Westphalia (figure 1). At each of these domains, simula-  
 204 tions with  $25 \times 25$  grid points will be performed where the central grid point including  
 205 the observational site is cut with all vertical layers. Each domain will be simulated from  
 206 1999 to 2015.

### 207 2.4 Implementation of the Phenology Scheme

208 A general logistic approach for annually changing phenology in CCLM is adapted  
 209 from the LPJ philosophy of the Lund-Potsdam-Jena Dynamic Global Vegetation Model

**Table 1.** Parameters of the newly implemented phenology model based on Knorr et al. (2010).

Symbol	Description	Units
$\Lambda$	leaf area index	-
$t, \Delta t$	time, time step	s
$r, p$	growth rate, shedding rate	days <sup>-1</sup>
$T_S$	soil surface temperature	°C
$\tau_m$	averaging time for temperature	s
$T, T_{on}$	phenology temperature, threshold	°C
$\Lambda_T$	LAI depending on temperature (and day length)	-
$\varphi$	latitude	rad
$\delta$	declination of the sun	rad
$t_d, t_{on}$	day length, threshold	h (hours)
$W_c, W_{max}$	water content, maximum available	m
$\tau_s$	averaging time for water availability	s
$\Lambda_W$	LAI with water dependence	-
$\Lambda_S$	LAI with smoothed water availability	-

210 (LPJ-DGVM) (Sitch et al., 2003; Smith et al., 2001) in the form

$$\frac{d\Lambda}{dt} = r\Lambda\left(1 - \frac{\Lambda}{\Lambda_{max}}\right) - p\Lambda, \quad (1)$$

211 where LAI is  $\Lambda$  and its maximum value is  $\Lambda_{max}$ , the growth rate is  $r$  and the shedding  
 212 rate is  $p$ . It is used in the LPJ as well as in JSBACH (Raddatz et al., 2007; Reick et al.,  
 213 2013). The latter is the component for land and vegetation of the MPI Earth System  
 214 Model (Giorgetta et al., 2013). The MPI regional climate model REMO-iMOVE (Jacob  
 215 & Podzun, 1997; Wilhelm et al., 2013), a new model version with dynamic vegetation  
 216 phenology of REMO, also uses this approach. We adapt the new phenology model for  
 217 grassland in CCLM based on the work by Knorr et al. (2010) and the developments by  
 218 Schulz et al. (2015).

219 All parameters used in the following equations are described in table 1 and *min/max*  
 220 are minimum and maximum values. To avoid leaf area indices higher than the maximum  
 221 values or lower than the minimum values, the higher or lower values are corrected to the  
 222 limitations given by the external data. The equations are implemented in the source code  
 223 of CCLM as a new module step-by-step starting with the dependence on temperature,  
 224 followed by the dependence on day length, and followed by the dependence on water avail-  
 225 ability. The new module is called prior to the land surface model TERRA-ML during  
 226 the model run of CCLM. In this way, the transpiration and all other influenced param-  
 227 eters are calculated with the new LAI.

#### 228 **2.4.1 Dependence on Temperature**

229 The first step is to implement the phenology depending exclusively on the temper-  
 230 ature. The air and surface temperature can change very fast but the vegetation needs  
 231 its time to react. Therefore, a phenology determining temperature  $T$  is introduced (Knorr  
 232 et al., 2010). It is defined as a temperature  $T$  depending on the soil surface temperature  
 233  $T_S$  of a past period, weighted exponentially (Knorr et al., 2010):

$$T(t + \Delta t) = T(t) \cdot e^{-\Delta t/\tau_m} + T_S(t) \cdot (1 - e^{-\Delta t/\tau_m}). \quad (2)$$

234 Following the work by Schulz et al. (2015) the past period is chosen to be  $\tau_m = 15$  days.  
 235 Now the leaf area index  $\Lambda_T$  depending on the temperature can be calculated as follows:

$$\Lambda_T(t + \Delta t) = \begin{cases} \Lambda_{max} - e^{-r\Delta t} \cdot (\Lambda_{max} - \Lambda_T(t)), & \text{if } T \geq T_{on} \\ \Lambda_{min} - e^{-r\Delta t} \cdot (\Lambda_{min} - \Lambda_T(t)), & \text{else} \end{cases}, \quad (3)$$

236 where the growth rate is chosen to be  $r = 0.07 \text{ days}^{-1}$  which is an empirically tuned  
 237 value and the shedding rate is the same  $p = r$  (Schulz et al., 2015). The results of sim-  
 238 ulations with this implementation are in the following denoted as ' $T'$ '. The threshold  
 239 of the temperature is commonly set to 0 or 5 °C (Piao et al., 2015). Following again Schulz  
 240 et al. (2015) it is set to  $T_{on} = 5 \text{ °C}$ .

#### 241 **2.4.2 Dependence on Day Length**

242 The day length at a specific location contributes to the timing of vegetation growth  
 243 and decay. The day length depends on the latitude  $\varphi$  and the declination  $\delta$  of the sun.  
 244 It is calculated as

$$t_d = \arccos(-\tan \varphi \cdot \tan \delta) \cdot 24 \text{ h} / \pi, \quad (4)$$

245 and is given in hours. Now the leaf area index  $\Lambda_T$  depending on the temperature and  
 246 the day length calculates as

$$\Lambda_T(t + \Delta t) = \begin{cases} \Lambda_{max} - e^{-r\Delta t} \cdot (\Lambda_{max} - \Lambda_T(t)), & \text{if } T \geq T_{on} \text{ and } t_d \geq t_{on} \\ \Lambda_{min} - e^{-r\Delta t} \cdot (\Lambda_{min} - \Lambda_T(t)), & \text{else} \end{cases} \quad (5)$$

247 To have a Central European growing period which lasts at the most from February to  
 248 October the threshold for the day length is set to  $t_{on} = 10 \text{ h}$ . The results of simulations  
 249 with this implementation are denoted as ' $TD'$ '.

#### 250 **2.4.3 Dependence on Water Availability**

251 The water available for the plant is mainly determined by the water content of the  
 252 soil. It influences the transpiration by plants (Gardner & Ehlig, 1963). The water avail-  
 253 ability is even more important for plant growth than the temperature (Woodward, 1987).  
 254 Therefore, water availability has to affect the LAI in the model appropriately. The wa-  
 255 ter availability is adapted from the Knorr et al. (2010) approach to the CCLM.

256 The water available for the plants is the soil water that can be reached with the  
 257 roots. This is calculated in the model using all soil layers within the root depth of the  
 258 vegetation and is called water content  $W_c$ . The maximum for the plant available water  
 259 content  $W_{max}$  is also needed to obtain the ratio of available to maximum water content.  
 260 It can be calculated as the difference between the field capacity  $FCAP$  and the perma-  
 261 nent wilting point  $PWP$ . With the help of these variables a water-dependent leaf area  
 262 index  $\Lambda_W$  is calculated with

$$\Lambda_W = \Lambda_T \cdot \frac{W_c}{W_{max}}. \quad (6)$$

263 This is implemented in the model through a smoothed minimum function (Knorr et al.,  
 264 2010):

$$\Lambda_S = \frac{\Lambda_T + \Lambda_W - \sqrt{(\Lambda_T + \Lambda_W)^2 - 4\eta\Lambda_T\Lambda_W}}{2\eta}, \quad (7)$$

265 where  $\Lambda_S$  is the smoothed water available leaf area index and  $\eta = 0.99$ . Finally, these  
 266 steps are combined with the equation of the dependence on temperature and day length.  
 267 The following equation gives the complete formulation of the leaf area index  $\Lambda$  depend-  
 268 ing on the temperature, the day length, and the water availability:

$$\Lambda(t + \Delta t) = \Lambda_T \cdot e^{-\Delta t/\tau_s} + \Lambda_S \cdot (1 - e^{-\Delta t/\tau_s}). \quad (8)$$

269 Results of simulations with all parts of the new phenology implemented are denoted as  
 270 ' $TDW'$ '.

### 271 **3 Results and Discussion**

#### 272 **3.1 Annual Cycle of LAI**

273 The mean annual cycle of LAI from 1999 to 2015 is shown in figure 2 for the three  
 274 experimental domains. The timing of the maximum LAI in the simulations is closest to

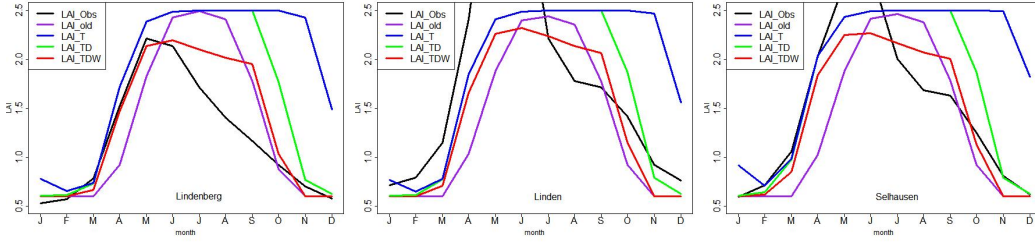


**Figure 2.** Mean (1999-2015) annual cycle of LAI. Results with the standard phenology (*\_old*, -), with only the dependence on temperature implemented (*\_T*, -), with the dependence on day length added (*\_TD*, -), with the fully implemented new phenology (*\_TDW*, -), and satellite observations (*\_Obs*, -) are shown at the three experimental domains Lindenberg, Linden, and Selhausen.

275 observations with the newly implemented phenology. The maximum value of LAI of the  
 276 standard simulations is reached in July whereas in the observations it is between May  
 277 and June. Implementing the dependence on temperature, the LAI stays at maximum  
 278 from June to November. Implementing additionally the dependence on day length, it fol-  
 279 lows the same mean annual cycle as with only the dependence on temperature except  
 280 for the earlier decrease in September. At the end of the growing season, the day length  
 281 threshold intervenes earlier than the temperature threshold. The water availability of  
 282 the complete newly implemented phenology reduces the LAI in summer which is why  
 283 the maximum value is between May and June, the same time of the year as in the obs-  
 284 servations. Also, the start of the growing season of the simulations with the newly im-  
 285 plemented phenology is in very good agreement with the observations. This applies to  
 286 all simulations except for those with the standard phenology. More details will follow  
 287 in the next section. However, the decrease of LAI starts later and faster in the simu-  
 288 lations compared to the observations but it ends at a similar time in the simulations (ex-  
 289 cept for the simulation only depending on temperature) and the observations.

290 Two differences remain between the simulations with the new phenology and the  
 291 observations (figure 2). The first one is the difference in the maximum value of LAI. It  
 292 is higher in the observations of Linden and Selhausen than in the simulations. This is  
 293 because the maximum value of LAI is fixed in the model through the external param-  
 294 eters. Another reason is that the satellite observations are related to different land-use  
 295 classes like urban areas, agriculturally used areas, and grassland, whereas in the simu-  
 296 lations all land-use classes are adjusted to grassland. The second difference between the  
 297 observations and the simulations can be found with LAI values from July to October up  
 298 to  $1\text{ m}^2/\text{m}^2$  higher in the simulations than in the observations. An explanation is the hu-  
 299 man impact through land use management. In Germany, the part of human used land  
 300 (agricultural, settlement, and transport area) is more than 65% (Umweltbundesamt, 2018).  
 301 Humans cut grass and harvest crops during summer and early autumn. This is the pe-  
 302 riod of the largest difference between the simulations and the observations in figure 2.  
 303 The human activities reduce the LAI in the observations, but this cannot be simulated  
 304 in CCLM because it is not a natural process. Those processes can not be represented  
 305 even in sophisticated models (Davin et al., 2014).

306 Correlation coefficients  $r$  between simulations and the observations are calculated  
 307 to evaluate the quality of the different simulations (table 2). Very high and significant  
 308 correlations are found for all simulations at the three stations. The highest correlation  
 309 coefficients are found between the simulations with the new phenology and the satellite  
 310 observations, followed by the simulations with the dependence on temperature and day

**Table 2.** Pearson’s correlation coefficient  $r$  for the monthly LAI of the different simulations from 1999 to 2015 compared to satellite observations, Fisher’s  $z$  for Pearson’s  $r$  of the standard simulation compared to the new phenology (in italic), and the  $p$ -value calculated from Fisher’s  $z$  (significant in bold).

	$r$ (LAI old~Obs)	$r$ (LAI T~Obs)	$r$ (LAI TD~Obs)	$r$ (LAI TDW~Obs)	$z$ (old~ TDW)	$p$ (Fisher)
Lindenberg	0.73	0.56	0.77	0.82	<i>-2.287</i>	<b>0.011</b>
Linden	0.67	0.51	0.71	0.77	<i>-2.101</i>	<b>0.018</b>
Selhausen	0.76	0.57	0.81	0.86	<i>-2.979</i>	<b>0.001</b>

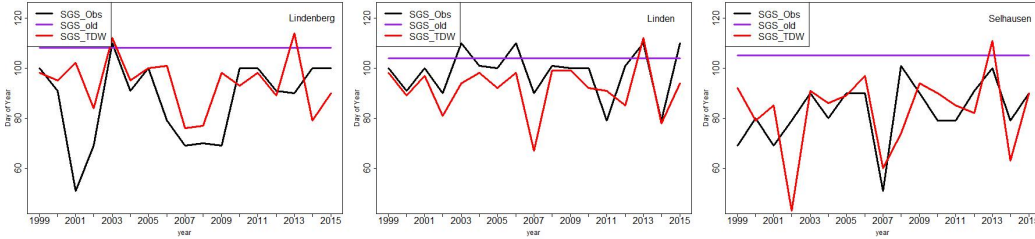


**Figure 3.** Start of the growing season (SGS) in number of days for each year from 1999 to 2015 and each domain (Lindenberg, Linden, and Selhausen) for satellite observations (*\_Obs, -*), the standard phenology simulations (*\_old, -*), and the new phenology simulations (*\_TDW, -*).

311 length of the new phenology, the standard phenology, and finally, the phenology only de-  
 312 pending on the temperature.

313 The improvement of the simulations compared to observations is quantified by Fisher’s  
 314  $z$ . The values and their probabilities for the comparison of the new phenology to the old  
 315 phenology are also shown in table 2. The improvement of the simulations from the stan-  
 316 dard to the new phenology is significant at all locations. More information to the sta-  
 317 tistical methods can be found in the appendix.

318 In summary, the mean annual satellite-observed cycle of LAI is represented most  
 319 accurately in the model with the newly implemented phenology. The representation of  
 320 LAI improved significantly compared to the standard phenology at all locations. In the  
 321 following section, we analyze the start of the growing season (SGS) of each year.

322 ***Start of the Growing Season***

323 The start of the growing season (SGS) is defined as the day when the LAI has reached  
 324 20 % of its maximum value (Murray-Tortarolo et al., 2013; Anav et al., 2013). In figure 3  
 325 the SGS is shown for the three domains in the satellite observations, the simulations with  
 326 the standard phenology, and the simulations with the new phenology. In the simulations  
 327 with the standard phenology, the SGS is constant because of the annually-recurring cycle.  
 328 The observations as well as the new simulations, have a large interannual variability  
 329 and are significantly positive correlated (Lindenberg  $r = 0.27$ , Linden  $r = 0.64$ ,  
 330 Selhausen  $r = 0.45$ ). For the majority of the years, the SGS of the simulations with the  
 331 standard phenology is approximately 2 months later compared to the observations and  
 332 the simulations with the new phenology (figure 3). This is because the phenology in the  
 333 standard simulation only depends on the latitude and altitude specifying the SGS at that

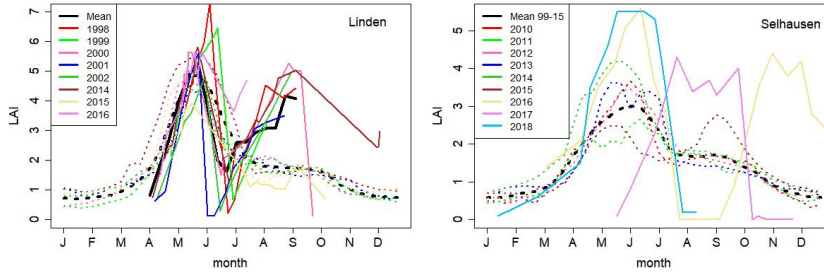


**Figure 4.** LAI satellite (dotted) and in-situ (lines) observations at Linden and Selhausen for the years shown in the legend on the left in different colors. In-situ measurements are only available for the given years and dates. At Linden, the shown simulated years are (except 1998) the same as the in-situ observations. At Selhausen, the six years of simulations before the in-situ observations are shown. The mean yearly cycle of the satellite LAI for the given years is shown in black (–).

334 date. When depending on temperature and day length in the new phenology module,  
 335 the SGS is earlier in spring and therefore closer to the observations.

336 In summary, the simulations with the newly implemented phenology with the inter-  
 337 terannual variability of SGS show the most similarity with the observations from satel-  
 338 lite data. The reliability of the satellite data is studied in the next section by compar-  
 339 ing the data to in-situ measurements.

#### 340 *Validation of Observations*

341 The stations Linden and Selhausen have in-situ measurements of the LAI. They  
 342 can be used to validate the satellite data with less precise results at a specific location  
 343 but constant horizontal and temporal resolution over a large domain and period (figure 4).  
 344 The in-situ measurements of LAI at Linden have two peaks per year because the grass  
 345 is cut twice a year. The first cutting is between the end of May and the beginning of June  
 346 showing the first decrease of LAI. The second cut is in September associated with the  
 347 second decrease of LAI. The satellite observation in the pixel including Linden shows the  
 348 first peak of LAI and a slightly increased value during the second peak of the in-situ mea-  
 349 surements. At Selhausen, the crops are harvested at a different time but only once each  
 350 year, hence the differences in the in-situ measurements of LAI in figure 4. In the satel-  
 351 lite observation over Selhausen, the first peak is nearly at the same time as over Linden.  
 352 It can also be seen in the in-situ measurements (2016: barley, 2018: winter wheat). The  
 353 second peak is also pronounced in the satellite observations but still with an only slightly  
 354 increased signal. At the same time, the peak appears in the in-situ measurements of 2017  
 355 (sugar beet) and later in 2016 (greening mix).

356 The major peak of the mean satellite observed LAI (figure 4) is in very good agree-  
 357 ment with the first peak of grass or the winter crops (e.g. barley, winter wheat) and the  
 358 minor peak is in good agreement with the second growth of grass or the summer crops  
 359 (e.g. sugar beet). That indicates a high percentage of human activities in the satellite  
 360 observations (cutting of grass and harvesting) (figure 4). Those human-induced, not nat-  
 361 ural processes are not part of the model. Hence, figure 2 shows differences between the  
 362 simulations and the observations. Differences in the annual cycle of LAI due to environ-  
 363 mental conditions are dealt with in the next section.

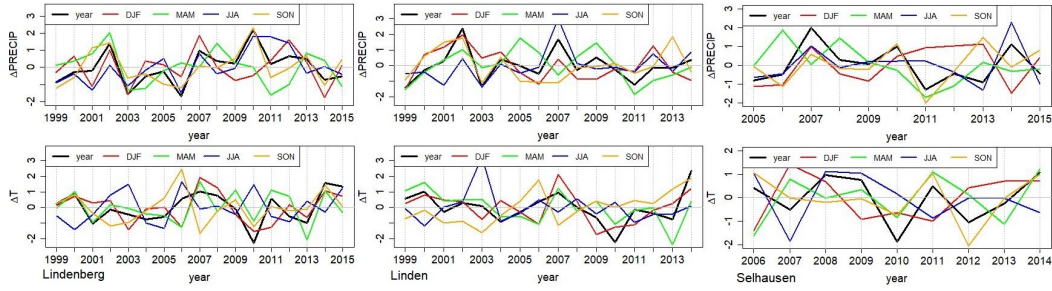


**Figure 5.** Standardized precipitation (top) and temperature (bottom) for each year of observations with the mean value in black, and the seasons winter (DJF, -), spring (MAM, -), summer (JJA, -), and autumn (SON, -) in different colors.

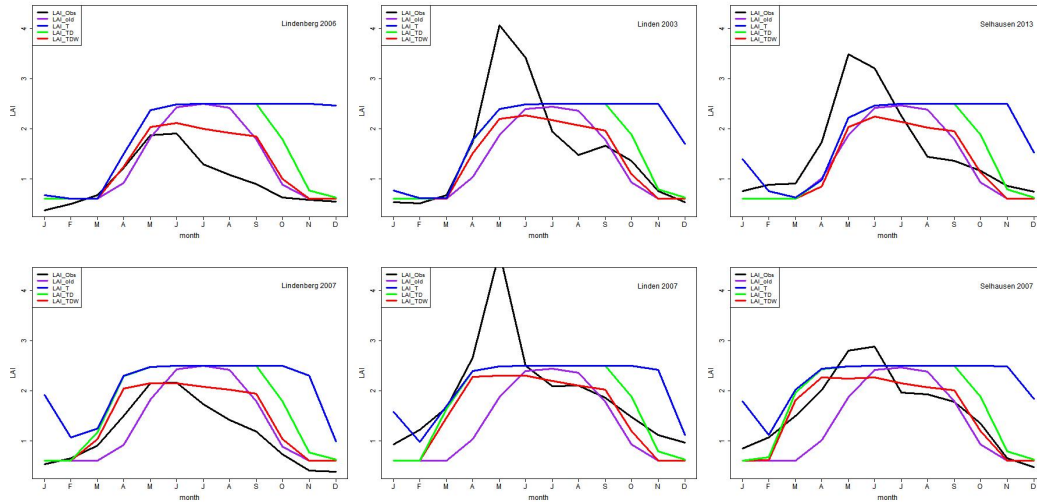


**Figure 6.** Annual cycle of LAI of the extremely dry years 2006 at Lindenberg, 2003 at Linden, and 2013 at Selhausen (top) and the year 2007 with extremely warm spring at Lindenberg, Linden, and Selhausen (bottom). In black (-) are the satellite observations (*\_Obs*) and in different colors the simulations with the standard phenology (*\_old*, -), with only the dependence on temperature (*\_T*, -), the dependence on temperature and day length (*\_TD*, -), and with the new phenology (*\_TDW*, -).

364

### *Influence of Temperature and Precipitation Extremes*

365

366

367

368

369

370

371

372

373

374

375

376

Figure 5 presents the standardized observed precipitation and temperature for the three experimental domains. The data is measured in-situ at different stations described in section 2.1. The drier the summer is the more the LAI is reduced due to water availability. The driest summers in figure 5 are 2006 at Lindenberg, 2003 at Linden and 2013 at Selhausen. The warmest winter and spring in figure 5 is 2007 at Lindenberg, Linden, and Selhausen. For the years with extreme events, the annual cycle of LAI is presented in figure 6. The satellite observations show a very sharp decrease in LAI during summer at all locations in the extremely dry years (upper panel of fig. 6). With the simulations including the dependence on water availability in red, the decrease of LAI starts at the same time as in the observations but is not as steep. The reduction due to water stress is improved compared to the simulations without dependence on water availability but is still limited by the thresholds. The improvement in the annual cycle of LAI of the ex-

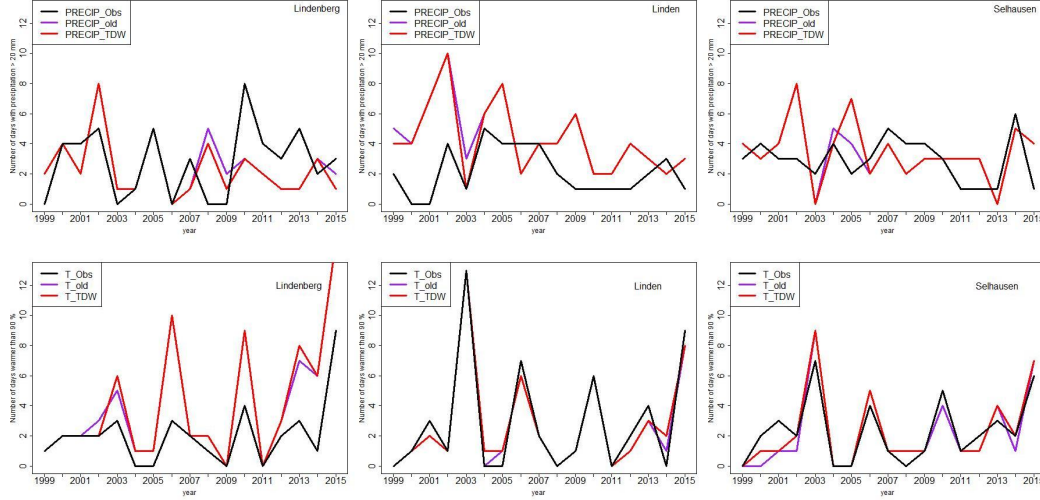


**Figure 7.** Heavy precipitation events with more than 20 mm per day (top) and very warm days within the 90th Percentile of the observed maximum temperatures (bottom) in each year of the period 1999 to 2015 at Lindenberg, Linden and Selhausen for the HYRAS observations (-Obs, -), the simulations with the standard phenology (-old, -) and the simulations with the new phenology (-TDW, -).

377 tre year 2007 is shown in the lower panel of figure 6. The winter and spring of 2007  
 378 were exceptionally warm with a strong impact on Germany’s phenology (Luterbacher  
 379 et al., 2007). The early SGS shown in the satellite observations can be simulated with  
 380 the newly implemented phenology because all simulations (.T, .TD, .TDW) show a clear  
 381 dependence on temperature. The standard phenology only depends on the latitude and  
 382 the altitude thus does not have an earlier SGS because of climatic conditions. Hence,  
 383 the SGS in those years is about two months later (figure 6 and figure 3).

384 In summary, we show that extreme temperature and precipitation events are in-  
 385 fluencing the annual cycle of LAI. In contrast to simulations with the standard phenol-  
 386 ogy module, CCLM can reproduce interannual variations in the annual cycle of the LAI  
 387 with the newly implemented phenology depending on surface temperature, day length,  
 388 and water availability.

### 389 3.2 Impacts of LAI

#### 390 *Impact on Precipitation and Temperature Extremes*

391 The influence of phenology on extreme precipitation and temperature (the oppo-  
 392 site of what was previously studied) is shown in figure 7. The simulations with the stan-  
 393 dard phenology and the new phenology are compared to the HYRAS gridded observa-  
 394 tional data set (Rauthe et al., 2013). Heavy precipitation events with more than 20 mm  
 395 precipitation on one day are shown in the upper panel of figure 7. The number of heavy  
 396 precipitation events is similar for all simulations and the observations at Lindenberg and  
 397 Selhausen. At Linden, the simulations have, on average, twice as much heavy precipi-  
 398 tation events as the observations. This could be due to the differences in land cover type  
 399 between reality and the modified grassland in the simulations. The total number of heavy  
 400 precipitation events in the simulations with the new phenology is closer to the observa-  
 401 tions in more years than with the standard phenology at Lindenberg and Linden and equal  
 402 at Selhausen.

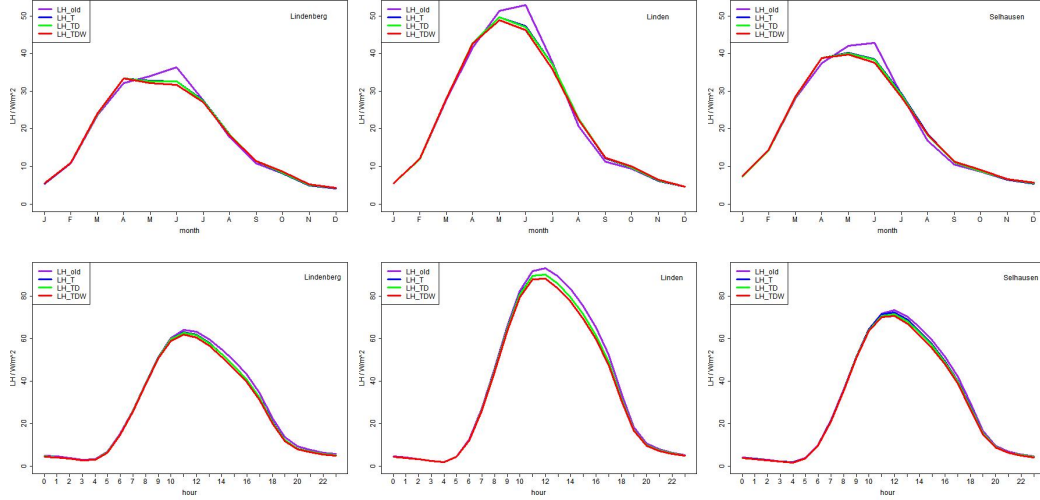


**Figure 8.** Mean (1999-2015) annual latent heat flux (top) and mean (1999-2015) daily latent heat flux during summer JJA (bottom) at Lindenberg, Linden and Selhausen for the simulations with the standard phenology (.old, -), with only the dependence on temperature (-T, -), the dependence on temperature and day length (-TD, -), and the simulations with the new phenology (-TDW, -).

403 The number of days within the 90th percentile of the maximum temperatures per  
 404 year can be seen in the bottom part of figure 7. The years with the most extreme warm  
 405 days are the same in the simulations and the observations. The correlation coefficients  
 406  $r$  between the simulations and the observations are with 0.89 for Lindenberg up to 0.99  
 407 for Linden very high. For Lindenberg, the average total number of days in the simula-  
 408 tions is twice as much as in the observations, again this may be due to the differences  
 409 in land cover type between the reality and the simulations. The average number of days  
 410 with the new phenology is generally closer to the observations than the number in the  
 411 simulations with the old phenology. The number of years, where the number of extremely  
 412 warm days fits better to the observations at Selhausen, is higher in the simulations with  
 413 the new phenology (figure 7).

414 In summary, simulations with the new phenology are more realistic regarding extre-  
 415 me events in precipitation and temperature because they fit better to the HYRAS ob-  
 416 servations than the simulations with the standard phenology. The influence of phenol-  
 417 ogy on the regional climate can also be seen in the transpiration, which is shown in the  
 418 following section.

419 ***Impact on Latent Heat Flux***

420 The vegetation also has a large impact on the latent heat flux due to transpiration.  
 421 Figure 8 (upper panel) shows the mean annual cycle of latent heat flux for the simula-  
 422 tions with different phenology calculations. In spring (March and April) and autumn (Au-  
 423 gust to October) the latent heat flux of the simulations with the new phenology is a few  
 424  $W/m^2$  higher. But in summer (May to July) the simulations with the old phenology are  
 425 up to  $5 W/m^2$  higher on average.

426 In summer, when the differences between the models are highest, the mean daily  
 427 cycle also differs. The lower panel of figure 8 shows the mean daily cycle of latent heat  
 428 flux for all summer days (June, July, and August) and all simulated years for the three  
 429 locations. The difference is highest during the daytime when the sun is at its zenith. Then

430 the influence of more vegetation in the simulations with the standard phenology is high-  
 431 est and transpires more what increases the latent heat flux. The simulations with the  
 432 new phenology have the lowest latent heat flux values in summer because of less vege-  
 433 tation. During nighttime when there is no solar radiation the latent heat flux is very low.

434 The expected influence of vegetation on latent heat flux (Yang et al., 1999; Peñuelas  
 435 et al., 2009) is shown in the simulations with the new phenology module. The latent heat  
 436 flux in summer is reduced because the LAI is also reduced due to the dependence on wa-  
 437 ter availability in the new phenology scheme. The lower LAI causes lower transpiration  
 438 and lowers latent heat flux. This causes lower humidity in the atmosphere and therefore  
 439 higher temperatures. The latent heat flux in summer is highest at Linden, followed by  
 440 Selhausen and Lindenberg. In general, radiation, precipitation, the climate type of the  
 441 area, and the vegetation type are found to be important factors for the evapotranspi-  
 442 ration (C. Williams et al., 2012). The type of vegetation and the climate type are pre-  
 443 defined in the simulations and the same at the three domains. Precipitation is highest  
 444 at Selhausen, followed by Linden and Lindenberg. This influences low latent heat fluxes  
 445 at Lindenberg. Radiation creates the remaining differences.

446 In summary, the influence of the phenology on the energy and water fluxes is shown  
 447 by the comparison of the latent heat flux simulated with the standard phenology and  
 448 with the newly implemented phenology. As expected, less vegetation in summer with the  
 449 new phenology leads to less latent heat. This also influences the representation of all re-  
 450 lated variables like humidity and temperature.

## 451 4 Conclusion

452 In this study, a new implementation of phenology in the COSMO-CLM model is  
 453 presented. The LAI as an indicator for phenology is calculated in the new module de-  
 454 pending on surface temperature, day length, and water availability. Simulations are per-  
 455 formed at three locations in Germany (Lindenberg, Linden, and Selhausen) from 1999  
 456 to 2015 with the standard phenology, with phenology depending on temperature, depend-  
 457 ing on temperature and day length and with the complete new phenology. The results  
 458 of the simulations with different calculation methods of LAI were compared with each  
 459 other and with observations. The questions in the introduction can be answered as fol-  
 460 lows:

- 461 1. How is the annual cycle of LAI affected by the newly implemented phenology?  
 462 The representation of the annual cycle of LAI significantly improved using the newly  
 463 implemented phenology compared to the standard phenology in CCLM. The tim-  
 464 ing of LAI including its increase, maximum, and decrease is closer to observations  
 465 with the new simulations. The interannual variability of the simulated SGS is more  
 466 consistent with the observations.
- 467 2. Does the representation of extreme events in CCLM change with the new phenol-  
 468 ogy module?  
 469 Extreme warm/dry years and their influence on phenology can be better resolved  
 470 with the new phenology in CCLM. The previously static annual cycle of LAI is  
 471 adjusted with the dependence on temperature and water availability to extreme  
 472 environmental conditions. On the other hand, the higher variability of LAI of the  
 473 newly implemented phenology shows a better representation of extreme precip-  
 474 itation and temperature events compared to the standard simulations with the annually-  
 475 recurring phenology. The number of heavy precipitation events per year and the  
 476 average number of extremely warm days have been improved.
- 477 3. What is the influence of the phenology on atmospheric variables, such as temper-  
 478 ature, precipitation, and moisture?  
 479 The newly implemented phenology causes changes in the energy and water cycle  
 480 of the model compared to the standard simulations. Lower LAI values (less vege-  
 481 tation) with the new phenology lead to less transpiration and latent heat flux,

482 resulting generally in lower humidity and higher temperature. Those differences  
 483 are small but especially in extreme years with less available water and higher tem-  
 484 peratures they are associated with a stronger positive feedback mechanism which  
 485 leads to less water and higher temperatures. The model with the standard phe-  
 486 nology does not show the interannual differences and therefore misses this effect.

487 The additional computational costs of the new phenology module are negligible and  
 488 it can be implemented easily. Considering this and the significant improvement it achieves,  
 489 the new phenology module will constitute a significant advance for CCLM. The newly  
 490 implemented phenology has interannual variability, which reveals changes in vegetation  
 491 due to climate change. The opposite effect of changes in phenology on climate change  
 492 can also be seen. Both processes are very important for predicting future climate change  
 493 with CCLM.

494 In summary, the LAI of the model, especially in summer, still needs enhancement  
 495 because the observations are highly influenced by human impact on vegetation (cutting  
 496 of grass, harvesting). Those human interventions in nature are not simulated in CCLM  
 497 and can therefore not be seen in the results. The next step is to simulate the phenology  
 498 for different vegetation types like deciduous and evergreen forest, summer and winter crop  
 499 over a larger domain in Central Europe.

## 500 Appendix A Statistical Methods

### 501 A1 Pearson Correlation

502 The pearson correlation coefficient or Pearson's  $r$  is used to measure the correla-  
 503 tion between two variables  $x$  and  $y$  (Pearson & Filon, 1898). It has values between +1  
 504 and -1 with  $r = 1$  means total positive linear correlation,  $r = 0$  means no linear cor-  
 505 relation, and  $r = -1$  means total negative linear correlation. Pearson's  $r$  is calculated  
 506 with

$$r = \frac{\text{cov}(x, y)}{\sigma_x \sigma_y}. \quad (\text{A1})$$

507 cov is the covariance of the two respective variables and  $\sigma_x$  and  $\sigma_y$  are the standard de-  
 508 viations. When comparing simulation results to observations the correlation is best the  
 509 closer  $r$  is to 1.

### 510 A2 Fisher Transformation

511 The Fisher transformation is used to compare two different pearson correlation co-  
 512 efficients (Fisher, 1925). With calculating  $z$  the relation of the different  $r$  values can be  
 513 estimated as follows

$$z = \frac{1}{2} \ln \left( \frac{1+r}{1-r} \right). \quad (\text{A2})$$

514 The probability  $p$  that the two correlations are related can be calculated with the con-  
 515 fidence interval around the Fisher's  $z$  (Eid et al., 2017). The smaller  $p$  the higher is the  
 516 probability that the two correlations are not related. This means if  $p < 0.05$  the dif-  
 517 ference is significant if  $p < 0.01$  the difference is very significant and if  $p < 0.001$  the  
 518 difference is highly significant.

### 519 A3 Standardization

520 The standardization is used to find the values that differ most from the average.  
 521 The standardized form  $z$  of a variable  $x$  is calculated as

$$z(x) = \frac{x - \mu}{\sigma}, \quad (\text{A3})$$

522 with the mean  $\mu$  and the standard deviation  $\sigma$ . The higher the absolute value of  $z$  the  
 523 more extreme is the variable  $x$ .

524 **Acronyms**525 **CCLM** COSMO-CLM526 **DWD** German Meteorological Service (Deutscher Wetterdienst)527 **LAI** Leaf Area Index528 **SGS** Start of Growing Season529 **Acknowledgments**

530 The authors acknowledge the German Meteorological Service (DWD) for providing ob-  
 531 servational data at the DWD Climate Data Center (CDC) and the HYRAS data. The  
 532 SPOT/PROBA-V LAI data product was generated by the land service of Copernicus,  
 533 the Earth Observation programme of the European Commission. The research leading  
 534 to the current version of the LAI product has received funding from various European  
 535 Commission Research and Technical Development programmes. The product is based  
 536 on SPOT/VGT 1km data ((c) CNES / PROBA-V 1km data ((c) ESA and distributed  
 537 by VITO), last access date: 28/9/2018. We acknowledge the GiFACE project at Lin-  
 538 den for producing the LAI and meteorological data at the Justus-Liebig-University Gießen.  
 539 We would like to thank the IBG-3 of the Forschungszentrum Jülich for providing us with  
 540 measurement data collected in the framework of the Transregional Collaborative Research  
 541 Center 32 (DFG) and the HGF initiative TERrestrial ENvironmental Observations (TERENO).  
 542 Computational resources were made available by the German Climate Computing Cen-  
 543 ter (DKRZ) through support from the Federal Ministry of Education and Research in  
 544 Germany (BMBF). We acknowledge the funding of the German Research Foundation  
 545 (DFG) through grant nr. 401857120.

546 **References**

- 547 Anav, A., Murray-Tortarolo, G., Friedlingstein, P., Sitch, S., Piao, S., & Zhu, Z.  
 548 (2013). Evaluation of land surface models in reproducing satellite Derived leaf  
 549 area index over the high-latitude northern hemisphere. Part II: Earth system  
 550 models. *Remote Sensing*, 5(8), 3637–3661.
- 551 Andresen, L. C., Yuan, N., Seibert, R., Moser, G., Kammann, C. I., Luterbacher, J.,  
 552 ... Müller, C. (2018). Biomass responses in a temperate European grassland  
 553 through 17 years of elevated CO<sub>2</sub>. *Global Change Biology*, 24(9), 3875–3885.
- 554 Baldauf, M., Seifert, A., Förstner, J., Majewski, D., Raschendorfer, M., & Rein-  
 555 hardt, T. (2011). Operational convective-scale numerical weather prediction  
 556 with the COSMO model: description and sensitivities. *Monthly Weather*  
 557 *Review*, 139(12), 3887–3905.
- 558 Baret, F., Weiss, M., Lacaze, R., Camacho, F., Makhmara, H., Pacholczyk, P., &  
 559 Smets, B. (2013). GEOV1: LAI and FAPAR essential climate variables and  
 560 FCOVER global time series capitalizing over existing products. Part1: Prin-  
 561 ciples of development and production. *Remote sensing of environment*, 137,  
 562 299–309.
- 563 Bartholy, J., & Pongrácz, R. (2007). Regional analysis of extreme temperature and  
 564 precipitation indices for the Carpathian Basin from 1946 to 2001. *Global and*  
 565 *Planetary change*, 57(1-2), 83–95.
- 566 Best, M., & Grimmond, C. (2016). Modeling the partitioning of turbulent fluxes  
 567 at urban sites with varying vegetation cover. *Journal of Hydrometeorology*,  
 568 17(10), 2537–2553.
- 569 Bogena, H., Montzka, C., Huisman, J., Graf, A., Schmidt, M., Stockinger, M., ...  
 570 Vereecken, H. (2018). The TERENO-Rur Hydrological Observatory: A multi-  
 571 scale multi-compartment research platform for the advancement of hydrological  
 572 science. *Vadose Zone Journal*, 17(1).

- 573 Camacho, F., Cernicharo, J., Lacaze, R., Baret, F., & Weiss, M. (2013). GEOV1:  
574 LAI, FAPAR essential climate variables and FCOVER global time series cap-  
575 italizing over existing products. Part 2: Validation and intercomparison with  
576 reference products. *Remote Sensing of Environment*, *137*, 310–329.
- 577 Chen, J., Menges, C., & Leblanc, S. (2005). Global mapping of foliage clumping in-  
578 dex using multi-angular satellite data. *Remote Sensing of Environment*, *97*(4),  
579 447–457.
- 580 Chmielewski, F.-M., & Rötzer, T. (2002). Annual and spatial variability of the  
581 beginning of growing season in Europe in relation to air temperature changes.  
582 *Climate research*, *19*(3), 257–264.
- 583 Collatz, G. J., Bounoua, L., Los, S., Randall, D., Fung, I., & Sellers, P. (2000). A  
584 mechanism for the influence of vegetation on the response of the diurnal tem-  
585 perature range to changing climate. *Geophysical Research Letters*, *27*(20),  
586 3381–3384.
- 587 Currie, P. O., & Peterson, G. (1966). Using growing-season precipitation to predict  
588 crested wheatgrass yields. *Journal of Range Management*, 284–288.
- 589 Cutini, A., Matteucci, G., & Mugnozza, G. S. (1998). Estimation of leaf area in-  
590 dex with the Li-Cor LAI 2000 in deciduous forests. *Forest Ecology and Man-  
591 agement*, *105*(1-3), 55–65.
- 592 Davin, E. L., Seneviratne, S. I., Ciais, P., Olliso, A., & Wang, T. (2014). Preferen-  
593 tial cooling of hot extremes from cropland albedo management. *Proceedings of  
594 the National Academy of Sciences*, *111*(27), 9757–9761.
- 595 Dee, D. P., Uppala, S. M., Simmons, A. J., Berrisford, P., Poli, P., Kobayashi, S., ...  
596 Vitart, F. (2011). The ERA-Interim reanalysis: Configuration and performance  
597 of the data assimilation system. *Quarterly Journal of the royal meteorological  
598 society*, *137*(656), 553–597.
- 599 Dickinson, R. E. (1984). Modeling evapotranspiration for three-dimensional global  
600 climate models. *Climate processes and climate sensitivity*, *29*, 58–72.
- 601 Doms, G., Förstner, J., Heise, E., Herzog, H., Mironov, D., Raschendorfer, M., ...  
602 Vogel, G. (2011). A Description of the Nonhydrostatic Regional COSMO  
603 Model. Part II: Physical parameterization. *Deutscher Wetterdienst, Offenbach,  
604 Germany*. (Available at <http://www.cosmo-model.org/>)
- 605 Eid, M., Gollwitzer, M., & Schmitt, M. (2017). *Statistik und Forschungsmethoden :  
606 mit Online-Materialien* (Vol. 5). Weinheim; Basel : Beltz, 2017.
- 607 Fisher, R. A. (1925). *Statistical methods for research workers* (Vol. 6). Oliver and  
608 Boyd, Edinburgh, Scotland.
- 609 Flerchinger, G., Kustas, W., & Wertz, M. (1998). Simulating surface energy fluxes  
610 and radiometric surface temperatures for two arid vegetation communities  
611 using the SHAW model. *Journal of Applied Meteorology*, *37*(5), 449–460.
- 612 Gardner, W., & Ehlig, C. (1963). The influence of soil water on transpiration by  
613 plants. *Journal of Geophysical Research*, *68*(20), 5719–5724.
- 614 Gilgen, A. K., & Buchmann, N. (2009). Response of temperate grasslands at dif-  
615 ferent altitudes to simulated summer drought differed but scaled with annual  
616 precipitation. *Biogeosciences Discussions*, *6*(3), 5217–5250.
- 617 Giorgetta, M. A., Jungclaus, J., Reick, C. H., Legutke, S., Bader, J., Böttinger, M.,  
618 ... Stevens, B. (2013). Climate and carbon cycle changes from 1850 to 2100 in  
619 MPI-ESM simulations for the Coupled Model Intercomparison Project phase 5.  
620 *Journal of Advances in Modeling Earth Systems*, *5*(3), 572–597.
- 621 González-Aparicio, I., & Hidalgo, J. (2012). Dynamically based future daily and sea-  
622 sonal temperature scenarios analysis for the northern Iberian Peninsula. *Inter-  
623 national journal of climatology*, *32*(12), 1825–1833.
- 624 Heide, O. M. (1974). Growth and dormancy in Norway spruce ecotypes (*Picea abies*)  
625 I. Interaction of photoperiod and temperature. *Physiologia Plantarum*, *30*(1),  
626 1–12.
- 627 Hodges, T. (1991). Temperature and water stress effects on phenology. *Predicting*

- 628 *crop phenology*, 7–13.
- 629 Jacob, D., & Podzun, R. (1997). Sensitivity studies with the regional climate model  
630 REMO. *Meteorology and Atmospheric Physics*, 63(1-2), 119–129.
- 631 Jameson, A., Schmidt, W., & Turkel, E. (1981). Numerical solution of the Euler  
632 equations by finite volume methods using Runge Kutta time stepping schemes.  
633 In *FLUID MECHANICS AND HEAT TRANSFER*. United States: NASA  
634 Center for Aerospace Information (CASI).
- 635 Jarvis, P. (1976). The interpretation of the variations in leaf water potential and  
636 stomatal conductance found in canopies in the field. *Philosophical Transactions  
637 of the Royal Society of London. B, Biological Sciences*, 273(927), 593–610.
- 638 Jeong, S.-J., HO, C.-H., GIM, H.-J., & Brown, M. E. (2011). Phenology shifts  
639 at start vs. end of growing season in temperate vegetation over the Northern  
640 Hemisphere for the period 1982–2008. *Global change biology*, 17(7), 2385–  
641 2399.
- 642 Jäger, H., Schmidt, S., Kammann, C., Grünhage, L., Müller, C., & Hanewald, K.  
643 (2003). The University of Giessen Free-Air Carbon Dioxide Enrichment study:  
644 Description of the experimental site and of a new enrichment system. *Journal  
645 of Applied Botany*, 77(5-6), 117-127.
- 646 Kammann, C., Grunhage, L., Gruters, U., Janze, S., & Jager, H. (2005). Response  
647 of aboveground grassland biomass and soil moisture to moderate long-term  
648 CO<sub>2</sub> enrichment. *Basic and Applied Ecology*, 6(4), 351-365.
- 649 Knorr, W., Kaminski, T., Scholze, M., Gobron, N., Pinty, B., Giering, R., & Math-  
650 ieu, P.-P. (2010). Carbon cycle data assimilation with a generic phenology  
651 model. *Journal of Geophysical Research: Biogeosciences*, 115(G4).
- 652 Kundzewicz, Z. W., Radziejewski, M., & Pinskiwar, I. (2006). Precipitation extremes  
653 in the changing climate of Europe. *Climate Research*, 31(1), 51–58.
- 654 Li-Cor, I. (1992). LAI-2000 plant canopy analyzer instruction manual. *LI-COR Inc.,  
655 Lincoln, Nebraska, USA*.
- 656 Luterbacher, J., Liniger, M. A., Menzel, A., Estrella, N., Della-Marta, P. M., Pfister,  
657 C., ... Xoplaki, E. (2007). Exceptional European warmth of autumn 2006 and  
658 winter 2007: Historical context, the underlying dynamics, and its phenological  
659 impacts. *Geophysical Research Letters*, 34(12).
- 660 Manabe, S. (1969). Climate and the ocean circulation: I. The atmospheric circu-  
661 lation and the hydrology of the earth's surface. *Monthly Weather Review*,  
662 97(11), 739–774.
- 663 Menzel, A., & Fabian, P. (1999). Growing season extended in europe. *NATURE*,  
664 397(6721), 659.
- 665 Merkel, A. O. P. A. (2020). *climate-data.org*. Retrieved 13.02.2020, from [https://  
666 de.climate-data.org/europa/deutschland/](https://de.climate-data.org/europa/deutschland/)
- 667 Murray-Tortarolo, G., Anav, A., Friedlingstein, P., Sitch, S., Piao, S., Zhu, Z., ...  
668 Zeng, N. (2013). Evaluation of land surface models in reproducing satellite-  
669 derived LAI over the high-latitude Northern Hemisphere. Part I: Uncoupled  
670 DGVMs. *Remote Sensing*, 5(10), 4819–4838.
- 671 Nagai, H. (2003). Validation and sensitivity analysis of a new atmosphere–soil–  
672 vegetation model. Part II: Impacts on in-canopy latent heat flux over a winter  
673 wheat field determined by detailed calculation of canopy radiation transmission  
674 and stomatal resistance. *Journal of Applied Meteorology*, 42(3), 434–451.
- 675 Neisser, J., Adam, W., Beyrich, F., Leiterer, U., & Steinhagen, H. (2002). Atmo-  
676 spheric boundary layer monitoring at the Meteorological Observatory Linden-  
677 berg as a part of the "Lindenberg Column": Facilities and selected results.  
678 *Meteorologische Zeitschrift*, 11(4), 241–253.
- 679 Oleksyn, J., Tjoelker, M., & Reich, P. B. (1992). Growth and biomass partitioning  
680 of populations of European *Pinus sylvestris* L. under simulated 50° and 60°N  
681 daylengths: evidence for photoperiodic ecotypes. *New Phytologist*, 120(4),  
682 561–574.

- 683 Oleson, K., Lawrence, D., Bonan, G., Drewniak, B., Huang, M., Koven, C., . . .  
684 Yang, Z.-L. (2013). *Technical description of version 4.5 of the Community*  
685 *Land Model (CLM)*. (Available at <http://www.cesm.ucar.edu/>)
- 686 Parmesan, C. (2006). Ecological and evolutionary responses to recent climate  
687 change. *Annual Review of Ecology Evolution and Systematics*, *37*, 637-669.
- 688 Parmesan, C., & Yohe, G. (2003). A globally coherent fingerprint of climate change  
689 impacts across natural systems. *NATURE*, *421*(6918), 37-42.
- 690 Pearson, K., & Filon, L. N. G. (1898). VII. Mathematical contributions to the the-  
691 ory of evolution.—IV. On the probable errors of frequency constants and on  
692 the influence of random selection on variation and correlation. *Philosophical*  
693 *Transactions of the Royal Society of London. Series A, Containing Papers of a*  
694 *Mathematical or Physical Character*(191), 229–311.
- 695 Peñuelas, J., Rutishauser, T., & Filella, I. (2009). Phenology feedbacks on climate  
696 change. *Science*, *324*(5929), 887–888.
- 697 Piao, S., Tan, J., Chen, A., Fu, Y., Ciais, P., Liu, Q., . . . Penuelas, J. (2015). Leaf  
698 onset in the northern hemisphere triggered by daytime temperature. *Nature*  
699 *Communications*, *6*, 6911.
- 700 Post, H., Hendricks Franssen, H.-J., Han, X., Baatz, R., Montzka, C., Schmidt, M.,  
701 & Vereecken, H. (2018). Evaluation and uncertainty analysis of regional-scale  
702 CLM4. 5 net carbon flux estimates. *Biogeosciences*, *15*(1), 187–208.
- 703 Raddatz, T., Reick, C., Knorr, W., Kattge, J., Roeckner, E., Schnur, R., . . . Jung-  
704 claus, J. (2007). Will the tropical land biosphere dominate the climate-carbon  
705 cycle feedback during the twenty-first century? *Climate Dynamics*, *29*(6),  
706 565–574.
- 707 Rauthe, M., Steiner, H., Riediger, U., Mazurkiewicz, A., & Gratzki, A. (2013). A  
708 Central European precipitation climatology—Part I: Generation and valida-  
709 tion of a high-resolution gridded daily data set (HYRAS). *Meteorologische*  
710 *Zeitschrift*, *22*(3), 235–256.
- 711 Reick, C., Raddatz, T., Brovkin, V., & Gayler, V. (2013). Representation of natu-  
712 ral and anthropogenic land cover change in MPI-ESM. *Journal of Advances in*  
713 *Modeling Earth Systems*, *5*(3), 459–482.
- 714 Reyes-Fox, M., Steltzer, H., Trlica, M., McMaster, G. S., Andales, A. A., LeCain,  
715 D. R., & Morgan, J. A. (2014). Elevated CO<sub>2</sub> further lengthens growing  
716 season under warming conditions. *NATURE*, *510*(7504), 259–262.
- 717 Richardson, A. D., Keenan, T. F., Migliavacca, M., Ryu, Y., Sonnentag, O., &  
718 Toomey, M. (2013). Climate change, phenology, and phenological control of  
719 vegetation feedbacks to the climate system. *Agricultural and Forest Meteorol-*  
720 *ogy*, *169*, 156–173.
- 721 Rockel, B., Will, A., & Hense, A. (2008). The regional climate model COSMO-CLM  
722 (CCLM). *Meteorologische Zeitschrift*, *17*(4), 347–348.
- 723 Ryder, J., Polcher, J., Peylin, P., Ottle, C., Chen, Y.-Y., van Gorsel, E., . . . Luys-  
724 saert, S. (2014). A multi-layer land surface energy budget model for implicit  
725 coupling with global atmospheric simulations. *Geoscientific Model Develop-*  
726 *ment Discussions*, *7*(1), 8649–8701.
- 727 Schnelle, F. (1955). *Pflanzen-Phänologie*. Akademische Verlagsgesellschaft Geest &  
728 Portig, Leipzig.
- 729 Schättler, U., & Blahak, U. (2017). A Description of the Nonhydrostatic Regional  
730 COSMO-Model. Part V: Preprocessing: Initial and Boundary Data for the  
731 COSMO-Model. *Deutscher Wetterdienst, Offenbach, Germany*. (Available at  
732 <http://www.cosmo-model.org/>)
- 733 Schulz, J.-P., Vogel, G., & Ahrens, B. (2015). A new leaf phenology for the land sur-  
734 face scheme TERRA of the COSMO atmospheric model. *COSMO Newsletter*,  
735 *15*. (Available at <http://www.cosmo-model.org/>)
- 736 Schulz, J.-P., Vogel, G., Becker, C., Kothe, S., Rummel, U., & Ahrens, B. (2016).  
737 Evaluation of the ground heat flux simulated by a multi-layer land surface

- 738 scheme using high-quality observations at grass land and bare soil. *Meteorolo-*  
739 *gische Zeitschrift*, 25(5), 607–620.
- 740 Settele, J., Scholes, R., Betts, R., Bunn, S., Leadley, P., Nepstad, D., . . . Taboad,  
741 M. (2014). *Terrestrial and inland water systems. In: Climate Change 2014:*  
742 *Impacts, Adaptation, and Vulnerability. Part A: Global and Sectoral Aspects.*  
743 *Contribution of Working Group II to the Fifth Assessment Report of the In-*  
744 *tergovernmental Panel on Climate Change* (C. Field et al., Eds.). Cambridge  
745 University Press, Cambridge, United Kingdom and New York, NY, USA. (pp.  
746 271–359)
- 747 Shen, M., Tang, Y., Chen, J., Zhu, X., & Zheng, Y. (2011). Influences of tem-  
748 perature and precipitation before the growing season on spring phenology in  
749 grasslands of the central and eastern Qinghai-Tibetan Plateau. *Agricultural*  
750 *and Forest Meteorology*, 151(12), 1711–1722.
- 751 Sitch, S., Smith, B., Prentice, I., Arneeth, A., Bondeau, A., Cramer, W., . . .  
752 Venevsky, S. (2003). Evaluation of ecosystem dynamics, plant geography  
753 and terrestrial carbon cycling in the LPJ dynamic global vegetation model.  
754 *Global Change Biology*, 9(2), 161–185.
- 755 Smets, B., Verger, A., Camacho, F., Van der Goten, R., & Jacobs, T. (2019). Coper-  
756 nicus Global Land Operations "Vegetation and Energy", PRODUCT USER  
757 MANUAL. *Issue 1.33 - version 2.* (Available at <https://land.copernicus.eu/>)
- 758 Smith, B., Prentice, I. C., & Sykes, M. T. (2001). Representation of vegetation  
759 dynamics in the modelling of terrestrial ecosystems: comparing two contrasting  
760 approaches within European climate space. *Global Ecology and Biogeography*,  
761 10(6), 621–637.
- 762 Stéfanon, M., Drobinski, P., d'Andrea, F., & de Noblet-Ducoudré, N. (2012). Effects  
763 of interactive vegetation phenology on the 2003 summer heat waves. *Journal of*  
764 *Geophysical Research: Atmospheres*, 117(D24).
- 765 Tiedtke, M. (1988). Parameterization of cumulus convection in large-scale models.  
766 In *Physically-based modelling and simulation of climate and climatic change*  
767 (pp. 375–431). Springer.
- 768 Tölle, M. H., Gutjahr, O., Busch, G., & Thiele, J. C. (2014). Increasing bioenergy  
769 production on arable land: Does the regional and local climate respond? Ger-  
770 many as a case study. *Journal of Geophysical Research: Atmospheres*, 119(6),  
771 2711–2724.
- 772 Umweltbundesamt. (2018). *Umwelt und Landwirtschaft 2018.*
- 773 Verger, A., Baret, F., & Weiss, M. (2014). Near real-time vegetation monitoring  
774 at global scale. *IEEE Journal of Selected Topics in Applied Earth Observations*  
775 *and Remote Sensing*, 7(8), 3473–3481.
- 776 Walther, G., Post, E., Convey, P., Menzel, A., Parmesan, C., Beebee, T., . . . Bair-  
777 lein, F. (2002). Ecological responses to recent climate change. *NATURE*,  
778 416(6879), 389–395.
- 779 Watson, D. J. (1947). Comparative physiological studies on the growth of field  
780 crops: I. Variation in net assimilation rate and leaf area between species and  
781 varieties, and within and between years. *Annals of botany*, 11(41), 41–76.
- 782 White, M., Thornton, P., & Running, S. (1997). A continental phenology model for  
783 monitoring vegetation responses to interannual climatic variability. *Global Bio-*  
784 *geochemical Cycles*, 11(2), 217–234.
- 785 Wilhelm, C., Rechid, D., & Jacob, D. (2013). Dynamic coupling of regional at-  
786 mosphere to biosphere in the new generation regional climate system model  
787 REMO-iMOVE. *Geoscientific Model Development Discussions*, 6, 3085–3135.
- 788 Williams, C., Reichstein, M., Buchmann, N., Baldocchi, D., Beer, C., Schwalm, C.,  
789 . . . Schaefer, K. (2012). Climate and vegetation controls on the surface water  
790 balance: Synthesis of evapotranspiration measured across a global network of  
791 flux towers. *Water Resources Research*, 48(6).
- 792 Williams, I. N., & Torn, M. S. (2015). Vegetation controls on surface heat flux par-

- 793 titioning, and land-atmosphere coupling. *Geophysical Research Letters*, *42*(21),  
794 9416–9424.
- 795 Woodward, F. I. (1987). *Climate and plant distribution*. Cambridge University  
796 Press.
- 797 Yan, Z., Jones, P., Davies, T., Moberg, A., Bergstrom, H., Camuffo, D., . . . Yang, C.  
798 (2002). Trends of extreme temperatures in Europe and China based on daily  
799 observations. *Climatic Change*, *53*, 355–392.
- 800 Yang, Z.-L., Dai, Y., Dickinson, R. E., & Shuttleworth, W. J. (1999). Sensitivity  
801 of ground heat flux to vegetation cover fraction and leaf area index. *Journal of*  
802 *Geophysical Research: Atmospheres*, *104*(D16), 19505–19514.